ELSEVIER

Cement & Concrete Composites 21 (1999) 197–204

Cement & Concrete Composites

Damage mechanics applied to concrete reinforced with amorphous cast iron fibers, concrete subjected to compression

Carl Redon [a,b,*], Jean-Louis Chermant [a]

[a] *Lermat, UPRESA CNRS 6004, ISMRA, 6, bd. Maréchal Juin, 14050 Caen Cedex, France*
[b] *LRM2C, ESITC Caen, 1, rue Pierre et Marie Curie, 14610 Epron, France*

Received 9 March 1998; accepted 12 November 1998

Abstract

The evolution of damage in compression, due to microcracking, is investigated in concrete reinforced by amorphous cast iron fibers and compared to damage in non reinforced concrete whose workability and strength were similar. As microcracking is anisotropic, two damage variables are defined, d_1 in the orientation of compression and d_2 in a perpendicular orientation. Damage values are calculated as a function of the loss of stiffness measured during loading-unloading cycles. Since the fiber arrangement is 2D (isotropic transverse), it is shown that damage is delayed in a reinforced concrete stressed in an orientation perpendicular to the fibers. On the other hand, due to fiber/concrete debonding, damage is greater when the compression is applied in an orientation parallel to the fibers. The damage behavior of the non reinforced concrete is intermediate.

Keywords: Fiber reinforced concrete; Amorphous cast iron fibers; Microcrack and fiber orientation; Compression behavior; Anisotropic damage

1. Introduction

Fibers are used to reinforce concrete and to prevent brittle failure as they delay crack opening through fiber pull-out and fiber bridging mechanisms [1–4]. However, at the material scale, prior to the formation of a main crack, do the fibers limit the loss of stiffness in the inelastic strain domain in uniaxial compression?

This paper deals with the damage arising in concrete reinforced by amorphous cast iron fibers. After a brief description of these fibers and concrete used, the experimental set-up for measurement of strains under cyclic compression is then described.

Based on a previous quantification of the microcracking in compression, given by automatic image analysis techniques, [5,6], a damage operator is defined. The damage mechanics equations are developed in order to establish the evolution of the damage variable depending on the isotropic transverse fiber orientation [5,7–9].

Finally, the behavior of the concrete reinforced with amorphous cast iron fibers (FRC) is analyzed in order to make suggestions on use of that material in a given structure.

2. Experimental details

2.1. FRC and concrete matrix compositions

The amorphous cast iron fibers used in this study are ribbon shaped: they are 30 mm long, 1.6 mm wide, 0.03 mm thick and belong to the family of metallic glass materials. They are produced by melt spinning which ensures a tempering rate about one million of degrees Celsius per second. They are composed of (Fe, Cr) 80% and (P, C, Si) 20% in mass. Immersed in HCl (0.1 N) and in $FeCl_3$ (0.4 N) for 24 h, no corrosion was observed in such fibers. Their specific surface area is about 10 m^2/kg. Their tensile strength range is between 1400 and 2300 MPa and their density is 7.2. [10,11].

The testing was intended to compare the loss of stiffness of the FRC to the evolution of damage in a pure concrete matrix, having a similar workability, and thus a similar compactness once hardened.

* Corresponding author. The University of Michigan, Department of Civil & Environmental Engineering, Room 2324, G.G. Brown Building, Ann Arbor, Michigan 48109-2125 USA. Tel.: 001 734 763 6832; fax: 001 734 764 4292; e-mail: agnan@engin.umich.edu

0958-9465/99/$ – see front matter
PII: S0958-9465(98)00052-3

The FRC and the pure concrete matrix are based on the same constituents: 425 kg/m^3 of CPJ CEM II/A 32.5R ordinary Portland cement and 944 kg/m^3 of 0/4 mm round washed sand.

The FRC incorporates 930 kg/m^3 of 6/10 mm crushed gravel and is mixed with a low amorphous cast iron fiber content: volume fraction = 0.5% (i.e. 36 kg/m^3). Indeed, mixing higher quantities of fibers with gravel is unachievable. The w/c (water to cement ratio) is equal to 0.4. A polymelamine superplasticizer amount was adjusted close to 0.4% (weight of solid content of superplasticizer related to the cement weight), in order to achieve an optimal compactness [12].

The formulation of the corresponding pure concrete matrix is slightly different as the fiber volume fraction is now replaced by gravel. Thus, 944 kg/m^3 of 6/10 mm crushed gravel is used. Moreover, the pure concrete matrix was mixed without superplasticizer and with a w/c ratio equal to 0.38 in order to achieve a workability close to that measured for the FRC in an LCL apparatus: 6–8 s.

2.2. Specimens

An FRC block and a pure concrete matrix block, both 450 × 450 × 450 mm^3 in size, were cast and then submitted to vibration parallel to the casting axis, during 50 s. 160 ϕ × 320 mm^3 cylindrical specimens for compression were cored in these blocks (Fig. 1). The specimen ends were straightened with high rotating speed (1500 rpm) oscillating diamond cutting tools under water.

If such cylinders had been cast instead of drilled, the fiber orientation would have been influenced by the wall effects of the molds. Then one would not have measured intrinsic material properties. [13,14]. Uniaxial compression tests have been conducted on 8 month old FRC and pure matrix to evaluate the damage evolution.

At this age, the compression strength of the FRC was 50 MPa in orientation 1 and 42 MPa in orientation 2. Whatever the orientation, the compression strength of the pure concrete matrix was 44 MPa.

2.3. Testing

The compression was applied between steel plates, in direct contact with the concrete, with a 3000 kN Schenck hydraulic actuator (Fig. 2).

In order to investigate the loss of stiffness of the pure concrete matrix and of the FRC during a monotonous loading in compression, a series of loading–unloading cycles was performed. The cycles were monitored by a strain control software, at a 60 μm/min displacement rate. For each loading cycle, the maximum strain level was chosen manually in order to reveal the most significant steps of the loss of stiffness. After each full unloading (cf. points c' on Fig. 8), a 15 min delay was maintained to allow strain recovery, in order to measure the evolution of the actual permanent strains (cf. points c on Fig. 8). Such loading–unloading cycles do not induce any fatigue effects as evidenced by the superposition of a monotonous load–displacement curve (Fig. 3).

Axial displacements, parallel to compression, were recorded as the average of the signals of three linear

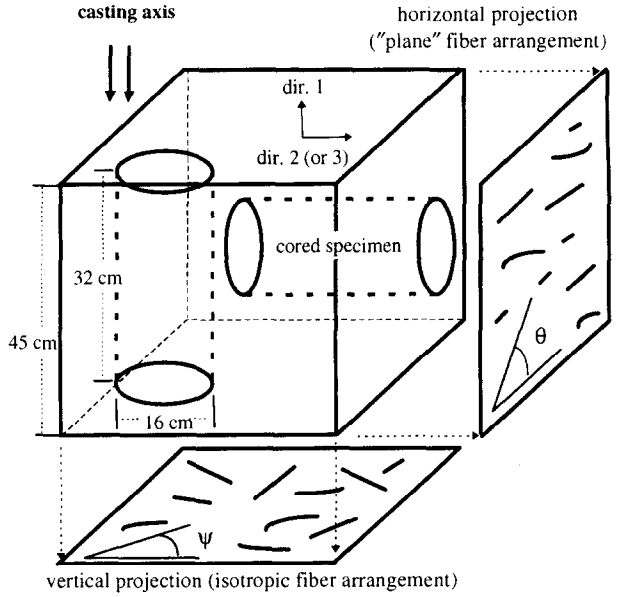

Fig. 1. Scheme of an FRC cube, of the cored specimens, and of the isotropic transverse fiber arrangement illustrated by two projected views.

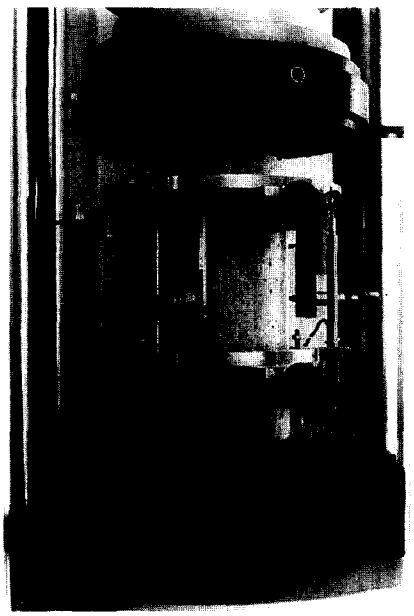

Fig. 2. View of the compression set-up and of the extensometer made of two aluminium rings used as the measure basis for the LVDTs.

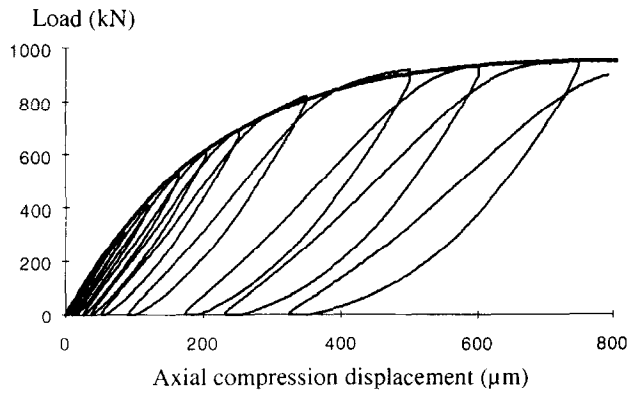

Fig. 3. Superposition of the load versus axial compression displacement curves for a 5 month old FRC: loading–unloading (thin line) and monotonous loading (thick line).

variable differential transducers (LVDT), having a ±10 mm range of measurement, and located at 120° around the specimen. Radial displacements were also measured as the average of the signals of three LVDTs perpendicular to the circumference of the specimen, having a range of measurement of ±1 mm, and also located at 120° around the specimen (Fig. 4). The LVDTs were placed on a measure basis constituted of two aluminium rings (Fig. 2), each positioned on the specimen with three spring contacts in order to eliminate the influence of radial strains on the measurement of the longitudinal displacements. Indeed, during loading, rigid contact would have indented the concrete surface and thus the rings, released during unloading, would have slipped down. One ring is independent of the other and the initial reference length between them is 185 mm. The initial reference length in the radial direction corresponds to the radius of the virgin specimen, 80 mm.

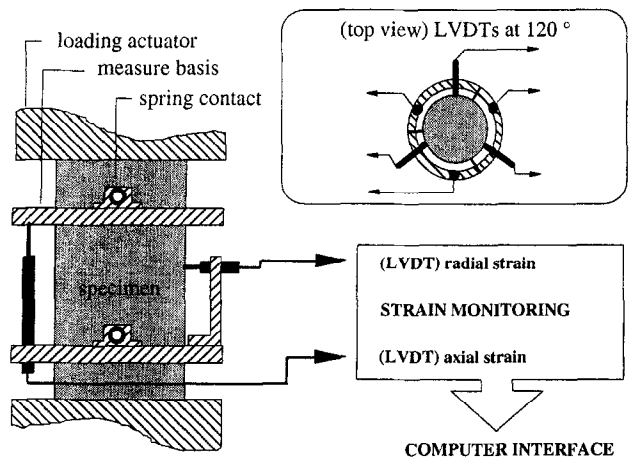

Fig. 4. Experimental set-up for the measurement of axial and radial displacements in loading–unloading conditions.

3. Results

3.1. Monotonic compression and comments on microcrack and fiber orientation

Automatic image analysis and Fourier transform, have been used to establish the rose of directions [15–17] of the fibers and of the microcracks at given strain levels.

On the one hand, it has been demonstrated that, due to the casting procedure, the amorphous cast iron ribbons arrangement is isotropic transverse (2D) in the hardened FRC [7]. Thus, the fibers can be considered as stratified in "planes" perpendicular to the casting axis (orientation 1), whereas their orientation is isotropic in these "planes" (orientation 2 and 3), (see Fig. 1).

On the other hand, similar to what can be observed in a pure concrete matrix, when the compression is applied either in orientation 1 or in orientation 2 (or 3), the microcrack network in the specimen is getting more and more anisotropic. It tends to be mainly oriented in the orientation of compression in both cases (Fig. 5) [5,7,18,19].

Thus, it seems that the fiber orientation has no significant effect on the microcrack orientation. The final microcrack orientation is rather dependent on the orientation of compression. So a damage variable d_1 has been related to damage in the axial orientation of compression, whereas d_2 characterizes damage in the radial orientations of the cored specimens [20].

3.2. Anisotropy of the compression behavior of the FRC

Compression tests have revealed that the FRC was mechanically isotropic in the elastic strain domain. The undamaged material is characterized by its A_0 stiffness matrix with two Young moduli, E_1, in orientation 1, E_2, in orientation 2 (or 3) and the corresponding striction coefficients γ_1 and γ_2.

But as damage due to microcracking appears (Fig. 5), the mechanical behavior of the FRC is inelastic and anisotropic. The example of a monotonous compression applied to a 9 month old FRC, shows that for a given axial deformation (Fig. 6), the corresponding radial displacement (Fig. 7) was larger if the FRC was stressed in orientation 2, which is parallel to the "planes" of fibers. Thus, even if microcrack orientation is roughly independent of the fiber orientation, this does not imply that fiber orientation has no effect on the loss of stiffness.

3.3. Damage mechanics

Based on Katchanov's theory [21], one uses a damage variable D [22], written here in a tensorial form (Eq. (1)) [20]. D relates the apparent stiffness matrix A – with apparent stiffness coefficients E_{*1} in orientation 1 and

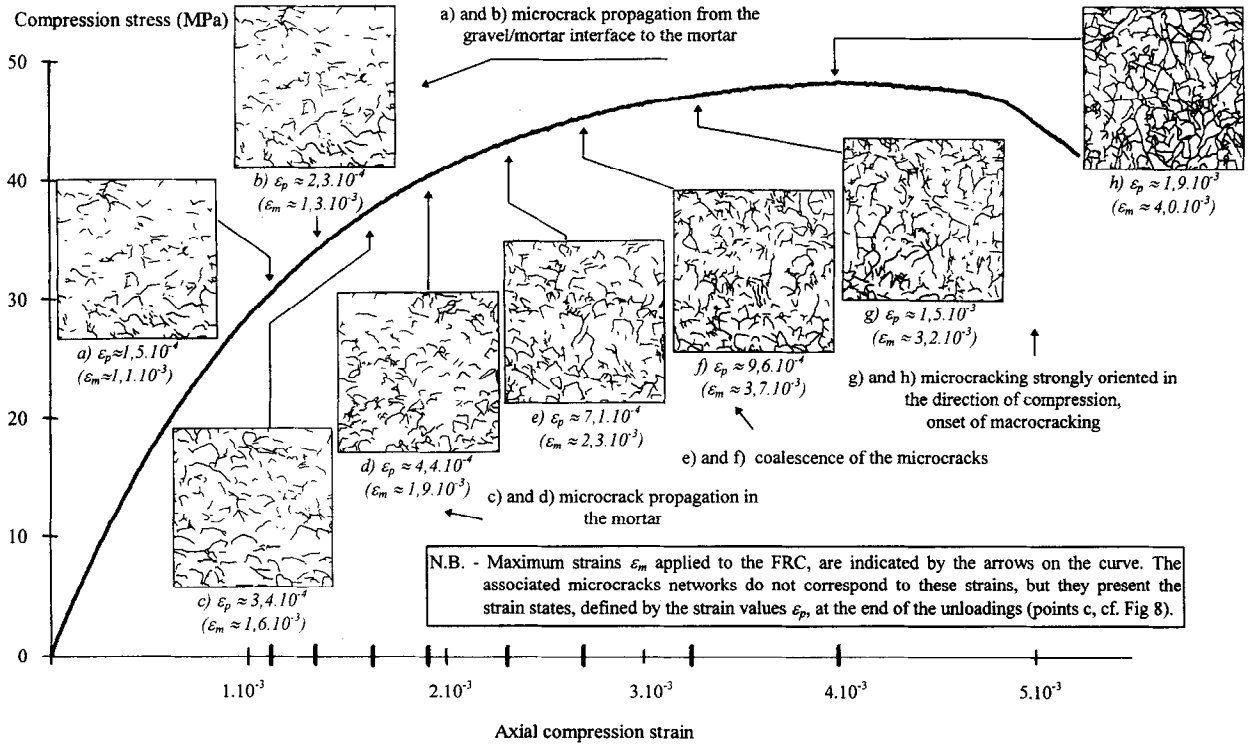

Fig. 5. Illustration of the successive steps of the microcracking process during the compression: case of a monotonous loading on a 9 month old FRC, stressed perpendicular to the "planes" of fibers. The microcrack patterns presented in the small images have been detected by a fluorescent resin under UV light at the surface of 10 × 10 cm² FRC slices.

E_{*2} in orientation 2 (or 3), and the corresponding apparent striction coefficients γ_{*1} and γ_{*2}, (Fig. 8) – of the damaged inelastic material, to the initial stiffness A_0 (Eq. (2)):

$$D = \begin{pmatrix} d_1 & 0 & 0 \\ 0 & d_2 & 0 \\ 0 & 0 & d_2 \end{pmatrix} \quad (1)$$

with: d_1, the damage variable in the orientation of compression (orientation 1 or 2 or 3),

d_2, the corresponding damage variable in the radial orientation of a specimen, perpendicular to the compression.

$$A(A_0, D) = M^{\mathrm{T}}(D) : A_0 : M(D) \quad (2)$$

D is equal to 0 as concrete is crack free and tends to 1 as the concrete specimen is split. It is supposed that the

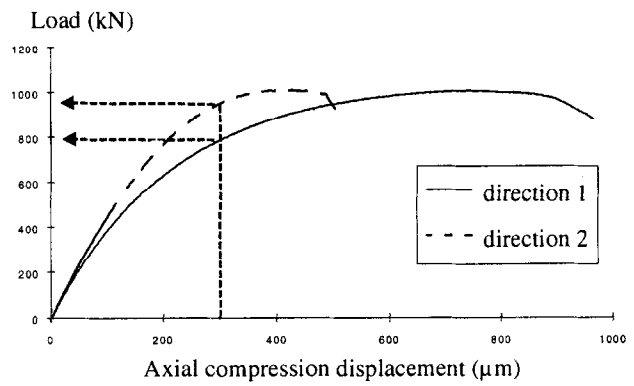

Fig. 6. Anisotropic compression behavior evidenced on monotonous load versus axial displacement curves for a 9 month old FRC.

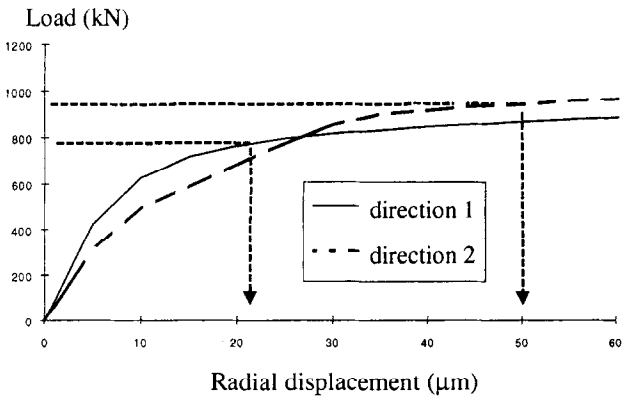

Fig. 7. Anisotropic compression behavior evidenced on monotonous load versus radial displacement curves, (corresponding to the same specimen as tested in Fig. 6) for a 9 month old FRC. The two arrows indicate that for the same given axial displacement, pointed out in Fig. 6, the corresponding radial displacement is larger in the case of the FRC stressed in orientation 2.

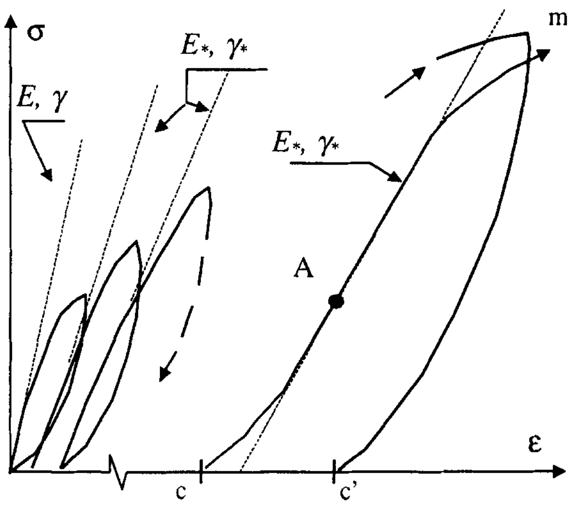

Fig. 8. Scheme for the measurement of stiffness slopes on a loading–unloading curve.

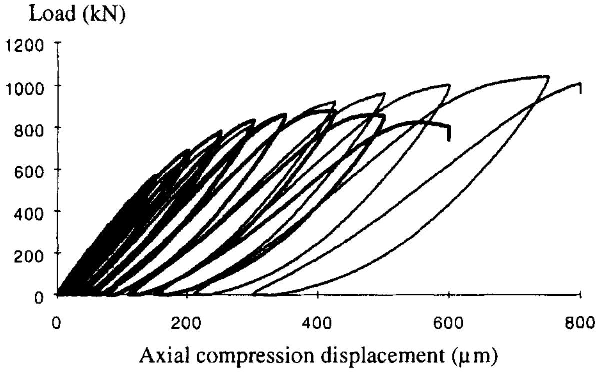

Fig. 9. Anisotropic diagram of load versus axial compression displacement for the 8 month old FRC in cyclic compression, tested in orientation 1 (thin line) and 2 (thick line).

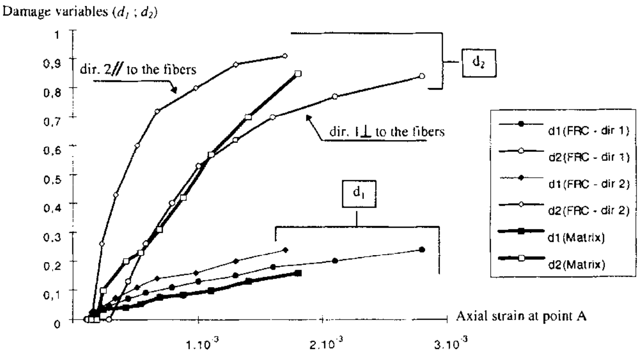

Fig. 10. Evolution of the damage variables, d_1 and d_2, as a function of the axial compression strain applied at the onset of the linear part of the loading cycles, for the 8 month old pure concrete matrix and for the 8 month old FRC tested in orientation 1 and in orientation 2 (or 3).

elastic strain energy, W_e, under an actual stress, σ, on a damaged cross section of the material is equivalent to the elastic strain energy due to the application of a so-called effective stress, σ_*, on the corresponding resistant crack-free cross section (Eq. (3)) [23,24]. One has:

$$W_e(\sigma, D) = W_e(\sigma_*) = \frac{1}{2}\overline{\overline{\sigma_*}}\colon A_0\left[\overline{\overline{\sigma_*}}\right]. \qquad (3)$$

Thus

$$\overline{\overline{\sigma_*}} = (I - D)^{1/2}\colon \overline{\overline{\sigma}}\colon (I - D)^{-1/2}$$

and

$$\overline{\overline{\varepsilon_{e*}}} = (I - D)^{1/2}\colon \overline{\overline{\varepsilon_e}}\colon (I - D)^{-1/2} \qquad (4)$$

with: $=$, the tensorial notation, M, the tensorial linear operator which conserves the symmetry of second order tensors, M^T, M transposed, I, the identity matrix, $\overline{\overline{\varepsilon_{e*}}}$, the effective elastic strain, $\overline{\overline{\varepsilon_e}}$ the actual elastic strain.

Using Eq. (2) and sets of (Eq. (4)), one writes either (Eq. (5))

$$\overline{\overline{\varepsilon_{e*}}} = A_0\overline{\overline{\sigma_*}} \quad \text{or} \quad \overline{\overline{\varepsilon_e}} = A\overline{\overline{\sigma}}. \qquad (5)$$

The loading–unloading curves corresponding either to axial or to radial displacements, and also revealing the anisotropic compression behavior of the 8 month old FRC, give then access to d_1 and d_2. These damage variables depend first on the initial stiffness E and γ, that we have calculated from the slope of the first loading cycle, (Fig. 8), and also on the orientation of compression (Fig. 9).

The evolution of the damage variables is also linked to apparent stiffness E_* and γ_*, determined on the linear part of the following loading cycles, once closure of the horizontal cracks, perpendicular to compression is finished. In Fig. 10, values of d_1 and d_2 are given for axial compression strains corresponding to the onset of the apparent linear elastic behavior of the damaged material (point A, see Fig. 8). Thus, the last strain value at the end of each damage curve does not correspond to a strain to rupture but rather to a critical strain indicating the onset of uncontrollable fracture. Practically indeed, it is not possible to obtain experimentally a value of D equal to 1.

(a) In the case of the matrix, from Eqs. (4) and (5), one has [20]

$$d_1 = 1 - \left(\frac{E_*}{E}\right)^{1/2} \quad \text{and} \quad d_2 = 1 - \left(\frac{v}{v_*}\right)\left(\frac{E_*}{E}\right)^{1/2}. \qquad (6)$$

(b) Similarly, in the case of the FRC stressed in orientation 1, one has [5]

$$d_1 = 1 - \left(\frac{E_{1*}}{E_1}\right)^{1/2} \quad \text{and} \quad d_2 = 1 - \left(\frac{\gamma}{\gamma_*}\right)\left(\frac{E_1}{E_{1*}}\right)^{1/2}. \qquad (7)$$

(c) Likewise, in the case of the FRC stressed in orientation 2, one has [5]

$$d_1 = 1 - \left(\frac{E_{2^*}}{E_2}\right)^{1/2} \text{ and } d_2 = 1 - \left(\frac{\gamma}{\gamma_*}\right)\left(\frac{E_2}{E_{2^*}}\right)^{1/2}. \quad (8)$$

3.4. Damage increase in the pure concrete matrix and in the FRC

The evolution of damage variables presented in Fig. 10, indicates that only d_2 constitutes a rupture criterion as it tends to 1. Thus the FRC as well as the pure concrete matrix, both 8 month old, failed due to radial microcrack openings, in an orientation perpendicular to the compression.

As compared to the pure concrete matrix, as shown on the d_2 curves, the onset of damage is delayed in the case of FRC stressed in orientation 1 – perpendicular to the "planes" of fibers (see Fig. 1). However, the onset of damage occurs sooner if the FRC is stressed in orientation 2 (or 3) – parallel to the "planes" of fibers.

As the strain level increases, the most progressive d_2 damage increase is recorded in the FRC stressed in orientation 1. Moreover, in that case, critical damage values, higher than 0.85 are reached for critical axial strains (2.8×10^{-3}) far larger than those of the pure concrete matrix and of the FRC stressed in orientation 2 (1.8×10^{-3}).

This means that fibers oriented in a parallel way to the compression do not enhance damage resistance. On the contrary, damage is even increasing faster in that case than in the corresponding pure concrete matrix.

Consequent to radial cracks opening, the loss of stiffness, given by d_1 increase, is also the largest in the FRC stressed in orientation 2.

The evolution of the permanent strains after unloading and recovery (points c on Fig. 8) as a function of the maximum applied load (points m on Fig. 8) confirms that the radial distortion is increasing faster in the FRC stressed in orientation 2 (or 3) than in orientation 1. The pure concrete matrix has an intermediate behavior (Fig. 11) [5].

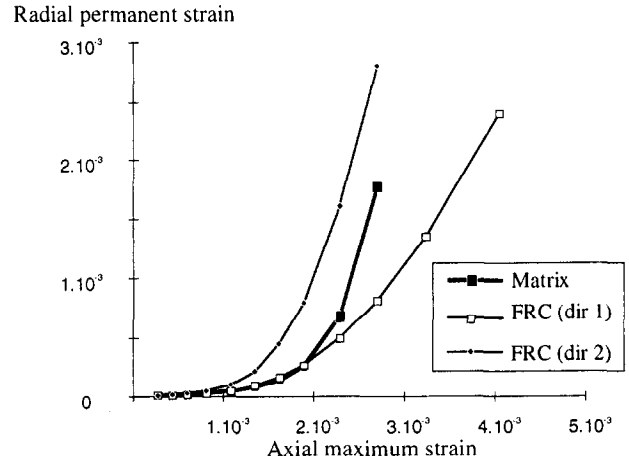

Fig. 11. Evolution of the permanent radial strains as a function of the maximum axial strain corresponding to the 3 tests related to Fig. 10, in the case of 8 month old FRC and pure concrete matrix.

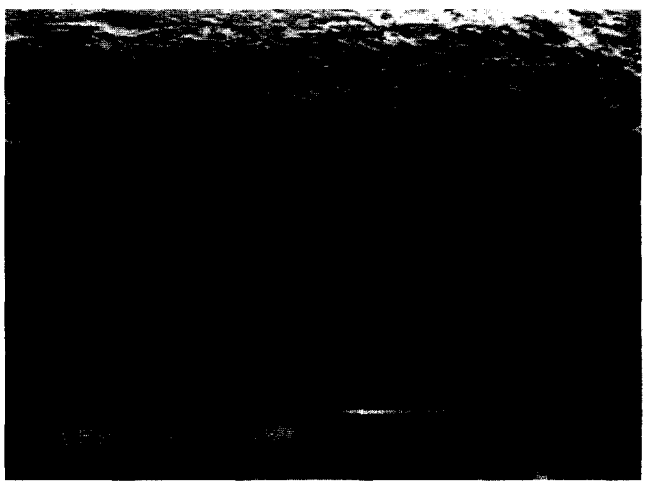

Fig. 12. SEM observation of portlandite and ettringite at the Fibraflex/cement interface.

4. Damage micromechanisms

In order to understand the difference in damage evolution when compression is parallel or perpendicular to the "planes" of fibers, it is necessary to have a look at the micromechanisms occurring in ITZ (Interface Transition Zones) along the fiber surface. The ITZ microstructure has been investigated at the surface of amorphous cast iron fibers pulled out from a mortar mixed with the same cement, sand and with a w/c = 0.5 [25].

It revealed large sheet-like portlandite, finger-like ettringite (Fig. 12) and very porous fibrillated CSH (Hydrated Calcium Silicate) crystals (Fig. 13). Under UV light, the impregnation of the microcracked FRC with a fluorescent resin, reveals that a fiber/matrix debonding mechanism is occurring in these ITZs which, as they are porous, are the weakest zones of the concrete (Fig. 14) [1,2,26].

Whatever the fiber orientation, the crack orientation is parallel to the axis of compression. As the amorphous cast iron fibers are ribbon-shaped, the ITZ are large.

Thus microcrack growth is promoted when the fiber, thus the ITZ, is aligned in the orientation of compression. This explains the faster d_2 damage increase observed in the FRC stressed in orientation 2 (or 3).

For the FRC compressed perpendicular to the "planes of fibers", the ITZ are no longer the most dangerous damage nucleation sites. Instead, a fiber microcrack bridging mechanism is counteracting

Fig. 13. SEM observation of porous fibrillated CSH at the Fibraflex/cement interface.

Fig. 14. Optical UV micrograph revealing fiber/concrete debonding in the FRC reinforced by Fibraflex fibers.

damage increase, involving fiber pull-out out of the crack faces [25].

5. Conclusion

The results obtained by automatic image analysis techniques, about the fiber and the microcrack orientations have constituted a basis for the study of the damage evolution in a concrete reinforced by amorphous cast iron fibers. It evidences, once more, the importance of morphological investigations to understand the mechanical response of materials, which is always related to their microstructure.

Either in a perpendicular or a parallel orientation to the "planes" of fibers, microcrack orientation does not depend on the 2D isotropic transverse fiber arrangement in the amorphous cast iron fiber-reinforced concrete. On the contrary, the microcracking orientation depends on

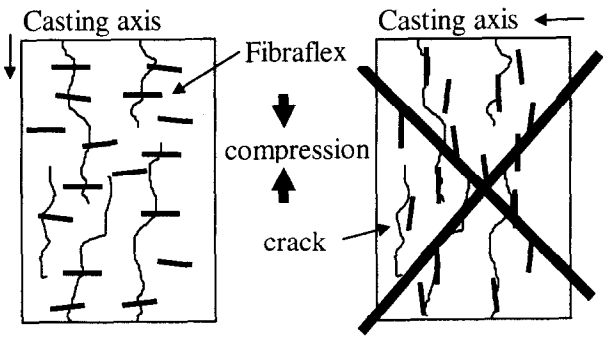

Fig. 15. Advice for use of Fibraflex FRC in a structure subjected to compression as a function of the fresh FRC mix casting direction: in the case on the left, damage will be delayed, whereas it will be favored in the case on the right.

the orientation of compression. As a result, microcracks are mainly oriented in the direction of compression.

But this does not imply that the fibers cannot counteract or delay microcrack opening. Delay has to be understood in terms of the amount of axial strain which has to be reached to achieve a given damage level. Then, as revealed by the loading-unloading tests, we have shown that, damage is delayed by a microcrack bridging process when fibers are perpendicular to the compression. This is essentially evidenced through the damage variable d_2, linked with radial microcrack openings perpendicular to the compression axis. Indeed, the increase of the d_2 value is the most progressive in this case. On the contrary, fiber/concrete debonding takes place in the interface transition zone when compression is parallel to the planes of fibers. The corresponding d_2 increase is then the fastest, the behavior of the pure concrete matrix being intermediate.

In fact, fiber orientation depends on the casting direction [7,8,14]. Thus, as it has already been indicated by Rossi and his colleagues [14], the casting procedure should be carefully chosen, depending on the orientation of solicitation for a given Fibraflex fiber-reinforced concrete structure, as shown in Fig. 15.

Acknowledgements

One of the authors (CR) wishes to thank the Partenariat ESTP-ESITC Caen and the Région de Basse-Normandie for their fellowship. We also wish to thank Mr. G. Peiffer, from Pont à Mousson SA (Pont à Mousson, France), supplier of the Fibraflex fibers.

References

[1] Brandt AM. In: Spon E & FN, editor. Cement-based Composites, Materials, Mechanical Properties and Performance. 1st ed. London: Chapman and Hall, 1995.

[2] Bentur A, Mindess S. Fiber Reinforced Cementitious Composites. Amsterdam: Elsevier, 1990.
[3] Zollo FR. Fiber-reinforced concrete: an overview after 30 years of development. Cement Concr. Comp. 1997;19(2):107–22.
[4] Li VC. Non-linear fracture mechanics of inhomogeneous quasi-brittle materials. In: Wunk MP, editor. Non Linear Fracture Mechanics, vol. 314. C.I.S.M., 1990;143 91.
[5] Redon C. Morphologie et comportement mécanique de bétons renforcés par des fibres de fonte amorphe. Thèse de Doctorat of the University of Caen, 1997.
[6] Redon C, Chermant L, Chermant JL. A mechanical damage model based on the measurement of microcrack orientation in concrete by Fourier transform. Acta Stereol 1997;16:287–92.
[7] Debicki G. Contribution à l'étude du rôle de fibres dispersées anisotropiquement dans le mortier de ciment sur les lois de comportement. Les critères de résistance et la fissuration du matériau. Thèse de Doctorat of the INSA of Lyon and of the University Claude Bernard Lyon I, 1988.
[8] Granju JL, Ringot E. Amorphous iron fiber reinforced concretes and mortars, comparison of the fiber arrangement. Acta Stereol. 1989;8:579–84.
[9] Redon C, Chermant L, Chermant JL, Quenec'h JL. Characterization of the macroporosity of concrete using an automatic image analysis. In: Brandt AM, Li VC, Marshall IH, editors. Proceedings of the International Symposium on Brittle Matrix Composites 5. Warsaw, Poland, 1997;291–99.
[10] De Gillebon B, Shom JM. Metallic glass ribbons – a new fibre for concrete reinforcement. Developments in Fibre Reinforced Cement and Concrete. University of Sheffield. Proceedings of the RILEM Symposium. 1986;12.
[11] Schacher B. Bétons et mortiers renforcés de fibres métalliques amorphes Fibraflex. Conchem, Karlsruhe, 1993;20.
[12] Redon C. Quenec'h JL, Chermant L, Chermant JL. Influence of superplasticizer and metallic glass ribbons on the macroporosity and the compressive strength in concrete. Acta Stereol. 1996;15:233–39.
[13] Stroeven P. Stereology of concrete reinforced with short steel fibres. Fract. Mech. Struct. Aspects. Concr. 1986;31:15–28.
[14] Rossi P, Harrouche N, Le Maou F. Comportement mécanique des bétons de fibres métalliques utilisées dans les structures en béton armé et précontraint. Ann. ITBTP, 479 bis série matériaux 1989;73:165–83.
[15] Serra J. Image analysis and mathematical morphology. New York: Academic Press, 1982.
[16] Coster M, Chermant JL. Précis d'analyse d'images. 2nd ed. Pans: Les Presses du CNRS, 1989.
[17] Redon C, Chermant L, Chermant JL, Coster M. Assessment of fibre orientation in reinforced concrete, using Fourier image transform. J. Microsc., 1998;19:258–265.
[18] Robinson GS. Methods of detecting the formation and propagation of microcracks in concrete. Cement and Concrete Association 1968:131–45.
[19] Stroeven P. Some aspects of the micromechanics of concrete. PhD thesis, TU Delft University, 1973.
[20] Bénouniche S. Modélisation de l'endommagement du béton hydraulique par microfissuration en compression. Thèse de 3ème Cycle of the University of Paris VI; 1979.
[21] Katchanov L. Rupture time under creep conditions. Izv. Akad. Nauk SSSR, OTN 1958;8:26–31.
[22] Lemaître J, Chaboche JL. Identification et classification rhéologique des solides réels. Mécanique des Matériaux Solides, Ch. 3. 1st ed. Dunod, 1988.
[23] Sidoroff F. Description of anisotropic damage application to elasticity. In: Hult J, Lemaître J, editors. Symposium IUTAM, Physical Non Linearities in Structural Analysis, Senlis. J. Phys. Appl. Mech. 1980;237–44.
[24] Cordebois JP, Sidoroff JP. Damage induced elastic anisotropy. Euromech 111, Marianske Lazne, 1978, Colloques Internationaux du CNRS, 1978;295:761–74.
[25] Redon C, Chermant JL, Quenec'h JL. Fiber pull-out tests and microstructure of fiber/mortar interface in fiber reinforced mortars. In: Brandt AM, Li VC. Marshall IH, editors. Proceedings of the International Symposium on Brittle Matrix Composites 5. Warsaw, Poland, 13–15 October 1997;64–73.
[26] Barnes BD, Diamond S, Dolch WL. Micromorphology of the interfacial zone around aggregates in Portland cement mortar. J. Am. Ceram. Soc. 1979;62:21–28.